

# Model Sub-tissue Morphological Components in mass spectrometry imaging data Using Dirichlet Gaussian Mixture Model

However, none of these methods can model the spatial morphology of single ion image.

In this paper, we proposed a new Dirichlet Gaussian Mixture model which incorporates spatial dependence to model single ion spatial distribution. In this model, the number of Gaussian components (spatial sub-structure) was automatically decided. It's straight forward to interpret the results of the model since it's single ion.

importance to class comparison. (Bag *et al.*, 2001) wants to know about ..... text follows.

Bofelli *et al.*, 2000 might want to know about text text text text (1)  
Bofelli *et al.*, 2000 might want to know about text text text text

## 2 Methods

$x^i, i = (1, 2, \dots, N)$ , denotes the ion intensity at pixel  $i$ .

$\pi^i = \pi_1^i, \dots, \pi_K^i$  denotes the prior probability of each component the  $i_{th}$  pixel belongs to.

$z^i = z_1^i, \dots, z_K^i$  denotes the discrete label of the  $i_{th}$  pixel.

$$z_j^i = \begin{cases} 1 & \text{if pixel } i \text{ belongs to component } j \\ 0 & \text{otherwise} \end{cases}$$

$$p(x^i) = \sum_{j=1}^K \pi_j^i p(x^i | \theta_j)$$

$$p(x^i) = \sum_{j=1}^K \pi_j^i p(x^i | \theta_j) p(\theta_j | \theta_{T_j})$$

$$p(x^i) = \sum_{j=1}^K \pi_j^i p(x^i | \theta_j) p(\theta_j | \theta_{T_j} + \gamma \theta'_{T_j})$$

$$p(x^i | \theta_j) = \frac{1}{(2\pi)^{1/2}} \exp\left(-\frac{1}{2}(x^i - \mu_j)^2 \sigma_j^{-1}\right)$$

The log-likelihood is:

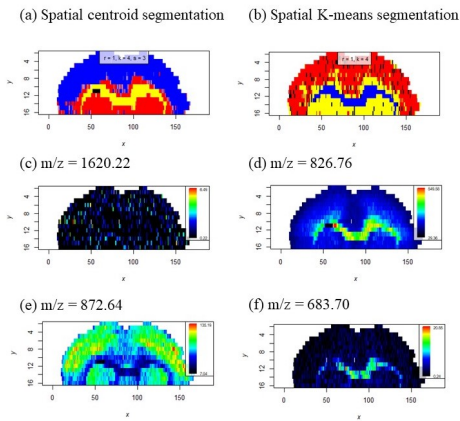


**Fig. 1.** MSI data of a mouse brain tissue. (a) spatial centroid segmentation results of 433  $m/z$ s; (b) spatial K-means segmentation results of 433  $m/z$ s; (c-f) sing ion image of  $m/z$  1620.22, 826.76, 872.64 and 683.70 respectively.

$$L(\Theta) = \sum_{i=1}^N \log \sum_{j=1}^K \pi_j^i p(x^i | \theta_j) + \log p(\Pi)$$

The discrete label  $z_j^i$  is a random variable following a multinomial distribution with  $M$  realizations.

$$p(z^i | \xi^i) = \frac{M!}{\prod_{j=1}^K (z_j^i)!} \prod_{j=1}^K (\xi_j^i)^{z_j^i}$$

in which  $(\xi_j^i) \geq 0$  and  $\sum_{j=1}^K \xi_j^i = 1$

The Dirichlet process is defined as:

$$p(\xi^i | \alpha^i) = \frac{\Gamma(\sum_{j=1}^K \alpha_j^i)}{\prod_{j=1}^K \Gamma(\alpha_j^i)} \prod_{j=1}^K (\xi_j^i)^{(\alpha_j^i - 1)}$$

In which,  $\alpha^i (\alpha^i > 0)$  is the vector of Dirichlet parameters.

$$p(z^i | \alpha^i) = \frac{M! \Gamma(\sum_{j=1}^K \alpha_j^i)}{\prod_{j=1}^K (z_j^i)! \Gamma(\sum_{j=1}^K (\alpha_j^i + z_j^i))} \prod_{j=1}^K \frac{\Gamma(\alpha_j^i + z_j^i)}{\Gamma(\alpha_j^i)}$$

$$\pi_j^i = p(z_j^i = 1 | \alpha^i) = \frac{\alpha_j^i}{\sum_{k=1}^K \alpha_k^i}$$

Incorporate the spatial dependence:

The posterior probability at iteration  $t$  is given by:

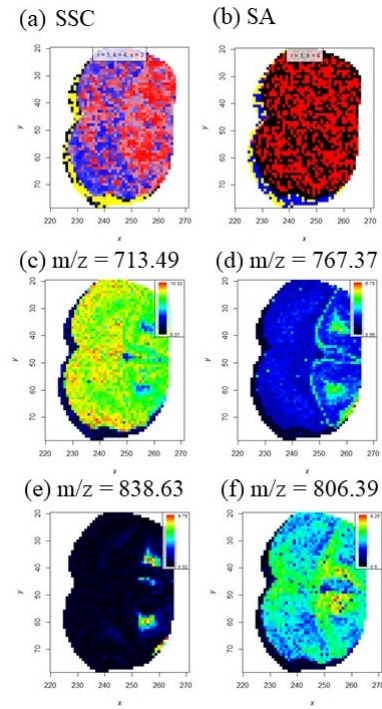


**Fig. 2.** MSI data of a mouse brain tissue. (a) spatial centroid segmentation results of 60  $m/z$ s; (b) spatial K-means segmentation results of 60  $m/z$ s; (c-f) sing ion image of  $m/z$  713.49, 767.37, 838.63 and 806.39 respectively.

$$y_j^{i(t)} = \frac{\pi_j^i p(x^i | \theta_j)}{\sum_{k=1}^K \pi_k^i p(x^i | \theta_k)}$$

To introduce the relationship between neighboring pixels, define

$$\bar{y}_j^i = \frac{1}{\sum_{m \subseteq N^i} d_m^i} \sum_{m \subseteq N^i} d_m^i y_j^{m(t-1)}$$

In which,  $d_m^i$  is the combination of spatial distance and spectrum similarity of two neighboring pixels, which can be written as:

$$d_m^i = \exp\left(\frac{(i-m)^2}{\sigma_1}\right) \exp\left(\frac{(S_i - S_m)^2}{\sigma_2}\right)$$

The new Dirichlet distribution is defined as:

$$p(\xi^i | \alpha^i) = \frac{\Gamma(\sum_{j=1}^K \alpha_j^i \bar{y}_j^{(i)\beta})}{\prod_{j=1}^K \Gamma(\alpha_j^i \bar{y}_j^{(i)\beta})} \prod_{j=1}^K (\xi_j^i)^{(\alpha_j^i \bar{y}_j^{(i)\beta} - 1)}$$

Therefore, the error function  $E(\Theta)$  is:

$$E(\Theta) = - \sum_{i=1}^N \sum_{j=1}^K y_j^{i(t)} \{ \log(\alpha_j^i \bar{y}_j^{(i)\beta}) - \log(\sum_{k=1}^K \alpha_k^i \bar{y}_k^{(i)\beta}) - \frac{1}{2} \log(2\pi) - \frac{1}{2} \log(\sigma_j^i) - \frac{1}{2} (x^i - \mu_j^i)^2 \}$$

In which,  $\Theta = (\mu_j, \sigma_j, \alpha_j, \beta)$

The objective is to  $\min_{\Theta} E(\Theta)$ .

In the M step,

$$\Theta^{(t+1)} = \Theta^{(t)} - \eta \nabla E(\Theta^{(t)})$$

In which  $\eta$  is the learning step. All  $\nabla E(\Theta^{(t)})$  has closed form and are subject to the constraints.

Bofelli *et al.*, 2000 might want to know about text text text text

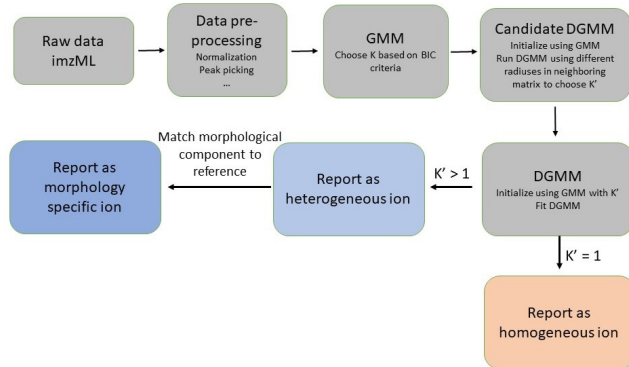


Fig. 3. flow chat sketch

### 3 Datasets

#### 3.1 Simulated Data

We simulated MSI datasets using function as below:

$$Y_i = \mu_{k(i)} + \phi_i + \epsilon_i$$

$$\phi_i \sim ICAR(\tau^2, W)$$

in which  $Y_i$  is the intensity of pixel  $i$ ,  $\mu_{k(i)}$  the mean intensity of sub-tissue morphological component  $k$  pixel  $i$  belongs to,  $\phi_i$  the spatial auto-correlation term and  $\epsilon_i$  the noise of pixel  $i$ .  $\epsilon_i$  follows intrinsic auto-correlation with variance  $\tau^2$  and  $W$  as neighboring matrix.

In the first dataset we simulated, all MSI images have identical morphologies but different noise levels. As shown in Fig XXXXX, All MSI have three morphological components: circle, triangle and the rest of image and the mean intensities of three morphological components are 100, 225, 150 respectively. The noise level varies from 5% of mean intensity to 32% of mean intensity. The variance for spatial auto-correlation is 25.

The second simulated data has 40 images or m/zs in total and every 10 m/zs have identical morphologies but different mean intensities for each morphological component. As shown in Fig XXXX, m/z 1-10 have three morphological components: circle, triangle and the rest of image, m/z 11-20 have two morphological components: triangle and the rest of image, m/z 21-30 have two morphological components: circle and the rest of image and m/z 31-40 have homogenous ion spatial distribution.

#### 3.2 Saline and CpG preconditioned mouse brain

CpG is an unmethylated oligodeoxynucleotide that has been shown to stimulate the toll-like receptor 9 and induce neuroprotection against ischemic damage. To estimate the metabolic changes on brains caused by CpG preconditioning, brain tissue sections of saline (control) and CpG preconditioned mice were collected and analyzed by nano-MSI experiment using a Thermo LTQ-orbitrap instrument via positive mode. The spatial resolution is approximately  $40 \times 200 \mu\text{m}$  and the mass range is 100-1500 Da. The original MSI data are in RAW format and converted to NetCDF format using Xcalibur software before read by Cardinal.

#### 3.3 Amyotrophic lateral sclerosis mouse brain

Amyotrophic lateral sclerosis is a neurodegenerative disease, 20% of which is caused by mutations of SOD1. Mice who expressing a human ALS mutation, Cu-Zn superoxide dismutase 1 become symptomatic after 130 days. Brain tissue sections of ALS mice and their non-SOD1/YFP littermates on day 150 were collected and analyzed by MALDI-MSI experiment using a solarix 9.4 T FTICR (Bruker Daltonics, Billerica, MA, USA) instrument via positive mode. The spatial resolution is  $100 \mu\text{m}$  and the mass range is 609.44-1400 Da. MALDI-MSI data were converted to imzML format before further processing using R.

### 4 Results and Discussion

In this section, we will first evaluate the performance of the proposed method in terms of estimation accuracy using simulated datasets and examine the performance of the proposed model to extract the morphological component from single ion images. Then we will discuss the potential applications of the proposed model in biomarker discovery, tissue classification and class comparison.

Bofelli *et al.*, 2000 might want to know about text text text text

Table 1. This is table caption

head1	head2	head3	head4
row1	row1	row1	row1
row2	row2	row2	row2
row3	row3	row3	row3
row4	row4	row4	row4

This is a footnote

4.1 Model performance

As shown in Fig XXXXX, for low noise level dataset, both GMM and DGMM can report the correct number of morphological components and have very low estimation error of the mean intensity of each morphological component and very low error of misclassifying pixels to morphological components. As the noise level increases, the morphological component image generated by GMM becomes very noise and the misclassification rate increases rapidly. However GMM model has much lower estimation error of the mean intensity of each component and misclassification rate comparing to GMM before noise level of 20% of mean. When noise level is above 20% of mean, the reported number of morphological components are not correct. The performance on reporting the correct number of morphological components depends on how distinguishable these components are. In general, for higher fold changes among mean intensities of components and lower noise level, DGMM have better performance. In this case, the mean intensity of the background component, circle component and triangle component have geometric 1.5 fold change and the noise tolerance is 20%.

Bofelli et al., 2000 might want to know about text text text text

4.2 Select Morphological Specific Ions

4.2.1 Identify ion of a heterogeneous distribution or homogeneous distribution

A critical important task in MSI data analysis is to identify  $m/z$  that have a heterogeneous distribution.  $m/z$  of a heterogeneous distribution is usually related to anatomic structure of tissue or lessions, thus it's of

great interest of further study. On the other hand, it's also important to evaluate whether ion has homogeneous distribution when it comes to drug delivery in clinical study. Although methods such as entropy analysis, texture analysis and morphometric analysis have been utilized to identify whether a  $m/z$  has homogeneous distribution, none of them is able to

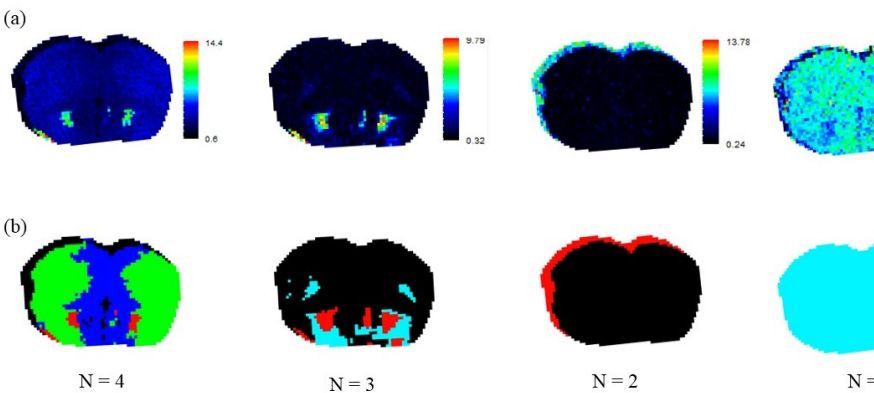


Fig. 5. Results of morphology modeled by DGMM (b) and the corresponding ion images (a)

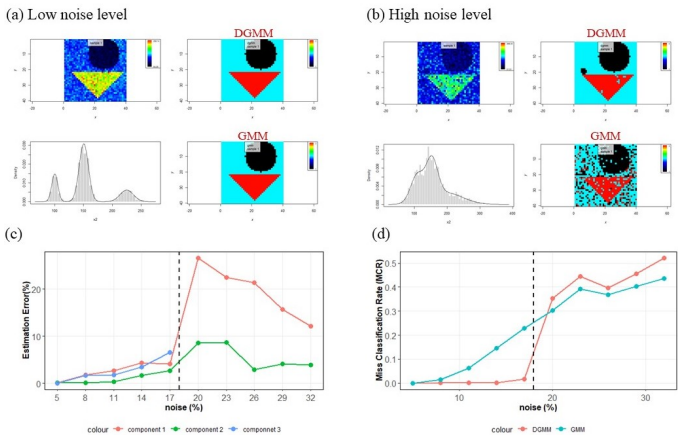


Fig. 4. Performance of DGMM on simulated dataset. (a) ion image (upper left), results of DGMM (upper right), histogram of ion intensities (lower left) and results of GMM(lower right) for low noise level data; (b) ion image (upper left), results of DGMM (upper right), histogram of ion intensities (lower left) and results of GMM(lower right) for high noise level data; (c) plot of estimation error of mean intensity of each morphological componnet vs noise level; (d) plot of misclassification rate vs noise level

provide the further information of spatial heterogeneity of each  $m/z$ . The proposed method can not only evaluate whether a  $m/z$  has homogeneous distribution and also provide the information of how many morphological components it has and the proportion and location of each components. (As shown in Fig XXXXXX) One can customize the minimum proportion of morphological components to ignore small hot areas based on respective research goal.

#### 4.2.2 Identify ion having a specific morphological component

Identifying  $m/z$  of a spatial pattern related to a specific area, which can be either an anatomic structure or an area of interest, is helpful to understand the molecular signature and potential pathways of sub-tissue structures. Using correlation coefficient between ion image of a  $m/z$  and binary matrix indicating a specific area is the most commonly used method to identify  $m/z$  co-localized in this area. It's fast and reliable when the ion is only depressed or over expressed in the specific area. However when the ion has multiple morphological components, using correlation coefficient is not able to identify these  $m/z$ s. Fig XXXXX shows that the correlation of ion image of  $m/z = XX$  is -0.51, which is comparatively low and similar to the correlation coefficient of ion image of  $m/z = XX$ . While we can see from the ion images that  $m/z = XXX$  has a more clear morphology of segment showing in Fig XXX(a). In this paper, we fit DGMM on ion images of distinct  $m/z$ s first, then match each morphological component to the segment showing in FigXXXX and select the morphological component of the highest matching score. The morphological component of highest matching score of 0.36 in ion image of  $m/z XXXX$  is the red area. The morphological component colored in black in ion image of  $m/z XXXX$  has a matching score of 0.78, which is distinguished from ion image of  $m/z XXXX$ .

Bofelli *et al.*, 2000 might want to know about text text text text

### 4.3 Clustering $m/z$ s with similar spatial patterns

Bofelli *et al.*, 2000 might want to know about text text text text

Clustering pixels of similar molecular profiles using whole mass spectrum has been studied using spatial aware K-means and spatial centroid segmentation method. However clustering  $m/z$ s of similar spatial patterns

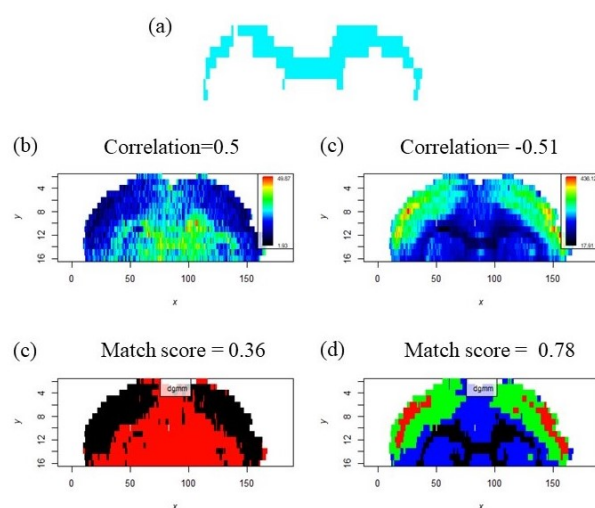


**Fig. 6.** (a) one segment generated by spatial centroid segmentation using 433  $m/z$ s which looks like corpus collarium; (b) ion image of  $m/z$  XXX; (c) ion image of  $m/z$  XXX; (d) morphological component modeled by DGMM;

have not been well studied. A naive way of doing this is to cluster  $m/z$ s based on the Euclidian distance between vectors of ion images. However the spatial information will be lost and it's very sensitive to the ion intensity. In Fig XXX, the simulated ion images of  $m/z$  1-10, 11-20, 21-30, 31-40 have identical spatial patterns respectively. The results of clustering based on Euclidian distance between vectors of ion images show that  $m/z$ s within each cluster do not have the same spatial patterns. Fig XX shows the results of clustering  $m/z$ s based on the Dice distance between vectors of morphological component labels and we can see that  $m/z$ s within the same cluster have identical spatial patterns.

#### 4.4 Morphological Component-Wise statistical analysis

- problems of averaging statistical analysis
- advantage of Morphological Component-Wise statistical analysis
- state of concept: real data example and simulation

## 5 Conclusion

(Table 1) Text Text Text Text Text Text Text Text Text Text Text Text  
Text Text Text Text Text Text Text Text Text. Figure 2 shows that the  
above method Text Text Text Text Text Text Text Text Text Text Text Text.  
Bofelli *et al.*, 2000 might want to know about text text text text Text Text  
Text Text Text Text Text Text Text Text Text Text Text Text Text Text Text  
Text Text Text Text. Figure 2 shows that the above method Text Text Text  
Text Text Text Text Text Text Text Text Text Text. Bofelli *et al.*, 2000 might  
want to know about text text text text Text Text Text Text Text Text Text  
Text Text Text Text Text Text Text Text Text Text Text Text Text Text Text.  
Figure 2 shows that the above method Text Text Text Text Text Text Text  
Text Text Text Text Text.

Text Text Text Text Text Text Text Text Text Text Text Text  
Text Text Text Text Text Text Text. Figure 2 shows that the above method  
Text Text Text Text Text Text Text Text Text Text Text Text. Bofelli *et al.*,  
2000 might want to know about text text text text

1. this is item, use enumerate
2. this is item, use enumerate
3. this is item, use enumerate

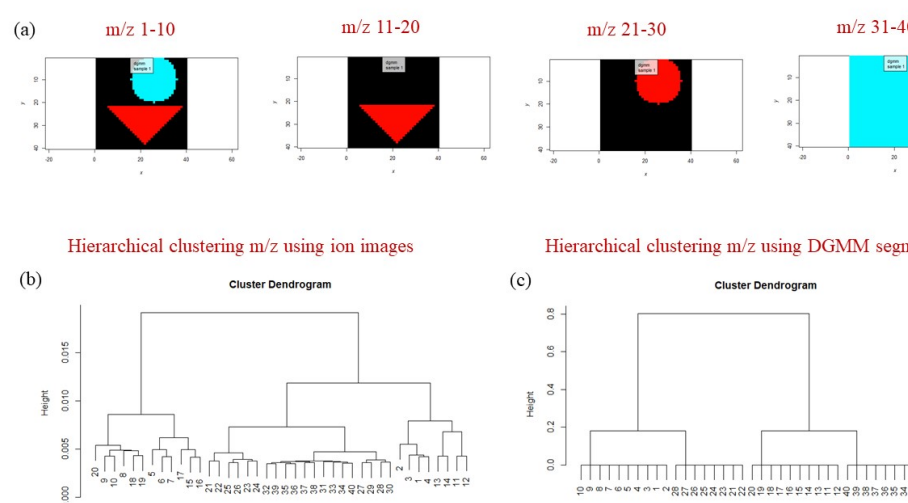


**Fig. 7.** clustering based on ion image and morphological component generated by DGMM

Text Text Text Text Text Text Text Text Text Text Text Text Text  
Text Text Text Text Text Text Text. Figure 2 shows that the above method  
Text Text Text Text

Text Text Text Text Text Text Text. Bofelli *et al.*, 2000 might want to know about text text text text

This work has been supported by the... Text Text Text Text.

Boffelli,F., Name2, Name3 (2003) Article title, *Journal Name*, **199**, 133-154.  
 Bag,M., Name2, Name3 (2001) Article title, *Journal Name*, **99**, 33-54.  
 Yoo,M.S. et al. (2003) Oxidative stress regulated genes in nigral dopaminergic neuron cell: correlation with the known pathology in Parkinson's disease. *Brain Res. Mol. Brain Res.*, **110**(Suppl. 1), 76–84.  
 Lehmann,E.L. (1986) Chapter title. *Book Title*. Vol. 1, 2nd edn. Springer-Verlag, New York.  
 Crenshaw, B.,III, and Jones, W.B.,Jr (2003) The future of clinical cancer management: one tumor, one chip. *Bioinformatics*, doi:10.1093/bioinformatics/btn000.  
 Auhutor,A.B. et al. (2000) Chapter title. In Smith, A.C. (ed.), *Book Title*, 2nd edn. Publisher, Location, Vol. 1, pp. ???–???.  
 Bardet, G. (1920) Sur un syndrome d'obesite infantile avec polydactylie et retinite pigmentaire (contribution a l'etude des formes cliniques de l'obesite hypophysaire). PhD Thesis, name of institution, Paris, France.